Proceedings of the 7th International Conference on HydroScience and Engineering

Philadelphia, USA September 10-13, 2006 (ICHE 2006)

ISBN: 0977447405

Drexel University

College of Engineering

VEGETATION TURBULENCE: FROM RANS MICRO-COMPUTATIONS TO MACRO-ANALYSIS

Dimitrios Souliotis[1] and Panayotis Prinos[2]

ABSTRACT

In this work turbulent flow in a vegetated channel is studied numerically for various submergence ratios and vegetation densities. The submergence ratio, H/h (H=flow depth, h=vegetation height) varies from 1.17 to 5.0 and the vegetation density α (α= A/V , A= frontal area of the cylinder and V= volume influenced by a single cylinder) from 2.46 to 4.3. The vegetation is considered rigid, simulated as cylindrical roughness and arranged in a staggered or a non-staggered pattern according to experimental data (Dunn et al., 1996 and Poggi et al., 2004). The 3D flow around a single cylinder is computed with the 3D RANS, a turbulence model of the k-ε type and appropriate boundary conditions. Based on detailed, "micro" flow characteristics (mean velocity, turbulent kinetic energy, shear stress etc.) the distributions of the respective "macro", spatial-averaged characteristics are analysed and are compared with respective experimental data (Dunn et al., 1996).
Implications for the macroscopic modeling of such flows are discussed and the significance of additional terms, resulting from volume-averaging, is analysed.

1. Introduction

There is a plethora of studies dealing with flow characteristics in vegetated channels. From a physical viewpoint, vegetation may be submerged or emerged, rigid or flexible with high or low density.

For the case of rigid vegetation the hydraulic behavior of the channel is similar to the behavior of a channel with macro-roughness which is caused by the presence of geometrical elements (cylinders, cubes etc.). For the second case the flexibility of the vegetation and the hydrodynamic of the flow contribute to the generation of several formations (erect, gently swaying, prone).

The ratio H/h (H=flow depth, h=vegetation height) characterizes the vegetation as submerged or emerged. With increasing values of the submergence ratio, H/h, the flow forcing within the vegetation

1 Phd Student, Hydraulics Laboratory, Department of Civil Engineering, Aristotle University of Thessaloniki, Thessaloniki, Greece (dsouliot@civil.auth.gr)
2 Professor, Hydraulics Laboratory, Department of Civil Engineering, Aristotle University of Thessaloniki, Thessaloniki, Greece (prinosp@civil.auth.gr)

changes from pressure-driven to stress-driven and the primary source of turbulence production shifts from stem wakes to the shear layer at the top of vegetation.

The methodologies used for studying the flow above and within vegetation are either experimental or numerical. Dunn et al. (1996) modelled the mean flow and the turbulence structure in open-channel flows with submerged vegetation and they compared the results with experimental observations. Poggi et al. (2004) examined, experimentally, the inter-connection between vegetation density and key flow statistics within and just above the vegetation. Nepf and Vivoni (2000) used laboratory experiments and they reveal two distinct flow zones within an aquatic canopy. The lower canopy, called the "longitudinal exchange zone" exchanges with surrouding water predominantly through longitudinal advection. The upper canopy, called the "vertical exchange zone" exchanges with surrouding water predominantly through vertical exchange. Huthoff and Augustijn (2006) used laboratory measurments in order to describe vegetation resistance and determine a way for including vegetation resistance in hydraulic models.

Experimental techniques, especially non-intrusive (LDA etc.), are quite satisfactory in cases of low vegetation density but are not applicable when vegetation is quite dense. However, some quantities (e.g. drag coefficient) are difficult to measure directly and their indirect estimation introduces errors in their magnitudes. In addition, due to limited point (local) measurements within the vegetation, the estimation of the respective volume (spatial) averaged quantities may not be accurate.

Numerical modeling of flow with vegetation is based on the volume (spatial) - averaged Reynolds Averaged Navier-Stokes (RANS) equations (Finnigan, 2000). The Volume-Average Theory (VAT) has been used for developing such equations (Whitaker, 1999). However additional turbulence terms in the resulting equations and especially in the turbulence model equations are modeled at an ad-hoc manner. A vegetative drag term is added to the momentum equations and additional turbulence production terms to the transport equations for the turbulence characteristics, usually k, ε, ω, when a turbulence model of the k-ε or k-ω type is used (Neary, 2003) or $-\overline{u_i u_j}$ when a Reynolds stress model is used (Choi and Kang, 2004). This results in non-satisfactory prediction of turbulence characteristics within the vegetative part of the flow for the case of submerged vegetation and especially near the top part of vegetation where the turbulence production is significant. Macroscopic models for porous media flow have been developed recently (Foudhil et al., 2005 and the references therein) but several drawbacks and limitations still exist. For example, the macroscopic modeling approach requires the turbulence modeling of the macroscopic turbulence and also a value for the drag coefficient C_d due to vegetation.

In this study, numerical modeling of flow is performed based on the 3D "microscopic" approach. Rigid, submerged vegetation in staggered and non-staggered array is investigated. The ratio H/h takes the values 1.17, 1.66, 1.82, 3.33 and 5. Computations of the 3D RANS equations in conjunction with a turbulence model of the k-ε type are performed in a unit cell, with appropriate vegetation densities, applying periodic conditions at the inlet and outlet of the computational domain. In order to obtain spatial- averaged (macroscopic) quantities, the computed microscopic results are subsequently averaged over planes parallel to the channel bed. In general, volume- averaged (macroscopic) quantities are calculated using the relationships: $\langle\psi\rangle = \frac{1}{V}\int_{V_f}\psi dV$ and $\langle\psi\rangle^f = \frac{1}{V_f}\int_{V_f}\psi dV$ where ψ=General fluid parameter, <ψ>= volumetric average (superficial), $<\psi>^f$= Intrinsic average (fluid). In the case of spatial-averaged quantities the volume is basically a plane, parallel to the channel bed, extensive enough to eliminate plant to plant variation in vegetation structure but thin enough to preserve the characteristic variation of properties in the vertical. Such an approach has several advantages over the other

approaches mentioned above. It allows the direct computation of C_d and also the accurate estimation of volume (spatial) averaged quantities since the latter are the result of detailed 3D computations.

2. Governing equations

2.1 Microscopic RANS and Numerical Procedure

The 3D RANS equations for steady, incompressible flow in conjunction with the standard k-ε model (Rodi, 1980), for calculating the turbulent stresses, are described as:

- Continuity equation

$$\frac{\partial U_i}{\partial x_i} = 0 \tag{1}$$

- Momentum equation

$$U_j \frac{\partial U_i}{\partial x_j} = -\frac{1}{\rho}\frac{\partial P}{\partial x_i} + \frac{\partial}{\partial x_j}\left[\nu\left(\frac{\partial U_i}{\partial x_j} + \frac{\partial U_j}{\partial x_i} \right) - \overline{u_i u_j} \right] \tag{2}$$

where U_i= time–averaged fluid velocity in the x_i direction, P= effective pressure (the difference between the static and the hydrostatic pressure), ρ= fluid density , ν= (μ/ρ)=fluid kinematic viscosity. For modelling the Reynolds stresses, $-\overline{u_i u_j}$, the eddy- viscosity concept is used:

$$\overline{u_i u_j} = \nu_t\left(\frac{\partial U_i}{\partial x_j} + \frac{\partial U_j}{\partial x_i} \right) - \frac{2}{3}\delta_{ij} k \tag{3}$$

where $\nu_t = C_\mu \frac{k^2}{\varepsilon}$ = eddy viscosity (C_μ =0.09), δ_{ij}= Kronecker delta, $k = \frac{1}{2}\overline{u_i^2}$ =turbulent kinetic energy.

The standard k-ε model (Rodi, 1980) is a semi- empirical model based on model transport equations for the turbulence kinetic energy (k) and its dissipation rate (ε). The turbulence kinetic energy and the dissipation rate are obtained from the following equations:

$$U_j \frac{\partial k}{\partial x_j} = \frac{\partial}{\partial x_j}\left(\frac{\nu_t}{\sigma_k}\frac{\partial k}{\partial x_j} \right) + \left(-\overline{u_i u_j}\frac{\partial U_i}{\partial x_j} \right) - \varepsilon \tag{4}$$

$$U_j \frac{\partial \varepsilon}{\partial x_j} = \frac{\partial}{\partial x_j}\left(\frac{\nu_t}{\sigma_\varepsilon}\frac{\partial \varepsilon}{\partial x_j} \right) + c_{\varepsilon 1}\frac{\varepsilon}{k}\left(-\overline{u_i u_j}\frac{\partial U_i}{\partial x_j} \right) - c_{\varepsilon 2}\frac{\varepsilon^2}{k} \tag{5}$$

where σ_κ, σ_ε $C_{\varepsilon 1}$, $C_{\varepsilon 2}$ =model constants (1.0, 1.3, 1.44, 1.92 respectively).

A steady k-ε model is used which does not account for the vortex shedding, generally present in flow around cylinders, and the associated momentum exchange and turbulence production, however its unsteady version would increase significantly the computational time and would require computational domain with no periodic conditions as it is described in the following paragraphs.

The segregated solver approach is used by which the governing equations are solved sequentially. Because the equations are non-linear (and coupled), several iterations of the solution loop must be performed before a converged solution is obtained. In the segregated solution method the discrete, non-linear governing equations are linearized to produce a system of equations for the dependent variables in every computational cell. The resultant linear system is then solved to yield an updated flow-field solution. The cases studied use the implicit form of linearization. By implicit we mean that for given variable, the unknown value in each cell is computed using a relation that includes both existing and unknown values from neighboring cells. Therefore each unknown will appear in more than one equation in the system, and these equations must be solved simultaneously to give the unknown quantities.

The FLUENT (6.0.12) CFD code (FLUENT Inc. 2001) is used which uses a control-volume technique to convert the governing equations to algebraic equations that can be solved numerically. This technique consists of integrating the governing equations about each control volume, yielding discrete equations that conserve each quantity on a control volume basis.

The discretized governing equation for a scalar quantity φ may be described as:

$$\sum_{f}^{N_{faces}} \rho_f \vec{u}_f \phi_f \cdot \vec{A}_f = \sum_{f}^{N_{faces}} \Gamma_f (\nabla\phi)_n \cdot \vec{A}_f + S_\phi V \qquad (6)$$

where N_{faces} = number of cell faces, ϕ_f = value of φ convected through face f, $\rho_f \vec{u}_f \cdot \vec{A}_f$ = mass flux through the face, $\vec{A}_f$ = area of face, $(\nabla\phi)_n$ = magnitude of $\nabla\phi$ normal to face f, V = cell volume. By default, the program stores descrete values of the scalar φ at the cell centers. However the face values φ_f are required for the convection terms in eq. (6) and must be interpolated from the cell center values. In this study for the pressure, momentum, Turbulence Kinetic Energy and Turbulence Dissipation Rate the second-order upwind scheme is used (FLUENT Inc. 2001). Pressure-velocity coupling, is achieved with the SIMPLE algorithm. Under-relaxation factors are used for controlling the change of φ. Typical values of under-relaxation factors, used in the study, are 0.3 for pressure, 0.7 for velocities and 0.8 for turbulence quantities.

3. Cases studied

The cases studied are based on experimental arrangements of Dunn et al. (1996) (Figure 1) and Poggi et al. (2004) (Figure 2). In these figures the boundary conditions are shown. For solid walls (channel bed and cylinders) Standard wall functions were used for both cases. The first is staggered and the latter is non-staggered. For each one of the above arrangements, flows with different submergence depth ratio were simulated while the plant density and bed slope were constant. The vegetation and flow characteristics are shown in tables 1 and 2. Regarding porosity, the value remains also constant for each arrangement. In all cases the porosity is very high.

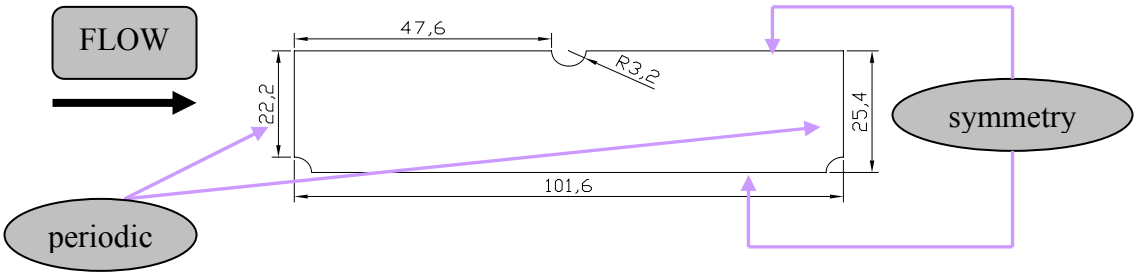

Figure 1: Plan view for the staggered case- Dunn et al. (1996)

Table 1: Flow characteristics (staggered cases)

Case	Plant density α (1/m)	Porosity φ	Bed slope So	Flow depth H (m)	Veg.Height h (m)	H/h
1	2.46	0.988	0.0036	0.1375	0.1175	1.17
2	2.46	0.988	0.0036	0.214	0.1175	1.82
3	2.46	0.988	0.0036	0.391	0.1175	3.33

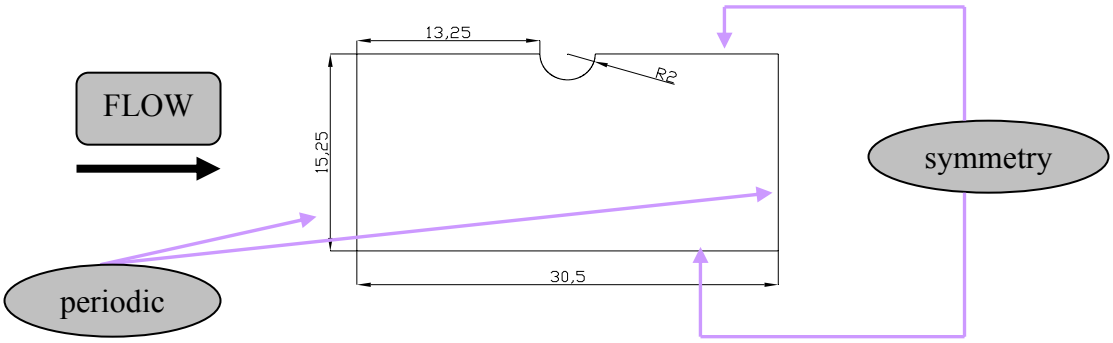

Figure 2: Plan view for the non-staggered case- Poggi et al. (2004)

Table 2: Flow characteristics (non-staggered cases)

Case	Plant density α (1/m)	Porosity φ	Bed slope So	Flow depth H (m)	Veg.Height h (m)	H/h
1	4.3	0.986	1.26e-04	0.2	0.12	1.66
2	4.3	0.986	1.26e-04	0.4	0.12	3.33
3	4.3	0.986	1.26e-04	0.6	0.12	5

For the construction of the grids the GAMBIT program was used. The grids were three-dimensional, structured and the shape of the cells was hexahedral. Also, the density of the grids was higher near the solid surfaces for estimating accurately the near-wall flow and turbulence characteristics. Finally the density of the grids inside the vegetative region was exactly the same.

For the staggered cases the computational cells varied between 33.000 and 76.000 depending on the value of H/h. Around the cylinder the number of nodes were 42, in the x-direction (flow direction) the nodes were 30, 34 and 62 for H/h=1.17, 1.82 and 3.33 respectively, in the z-direction the nodes were 14 and in the y-direction (normal to the bed) the nodes were 49, 55 and 65 for H/h=1.17, 1.82 and 3.33 respectively. Similarly, for the non-staggered cases the number of the computational cells was varied between 56.000 and 80.000 due to the higher values of H/h. Around the cylinder the number of nodes were 40, in the x-direction (flow direction) the nodes were 20 for all the cases, in the z-direction the nodes were 10 and in the y-direction (normal to the bed) the nodes were 85, 90, 130 for H/h=1.66, 3.33 and 5 respectively. The computational domain with the grid used is shown in figure 3 for both cases.

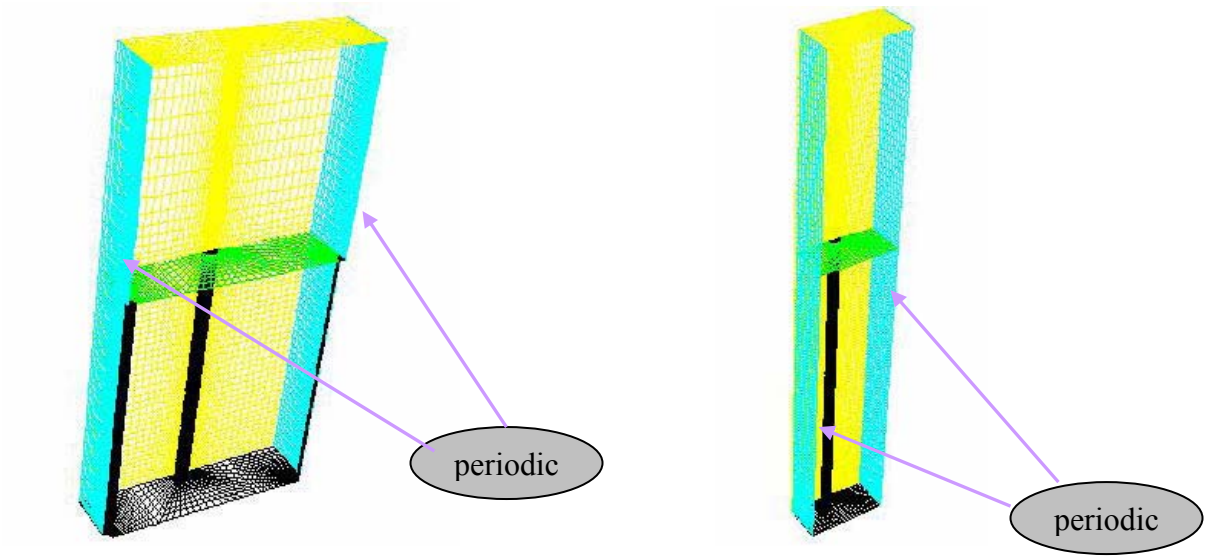

Figure 3: Computational domain and grid used (a) staggered, (b) non-staggered

In figure 4 details of the grid used at characteristic horizontal and vertical planes are shown.

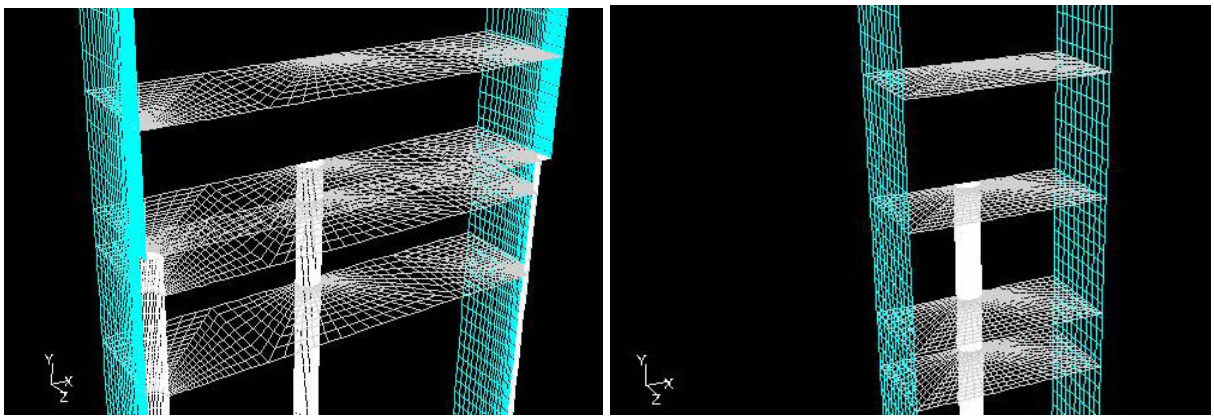

Figure 4: Detailed grid at characteristic planes

4. Analysis of results

In this section computed results are analyzed as directly derived from the computational 3D code (microscopic level). Also, spatial-averaged flow characteristics (macroscopic level) are presented and analyzed and finally the Boussinesq approximation for the spatial average shear stress ($<-\overline{uv}>$) is tested as well as the relationship for calculating $<\nu_t>$ from <k> and <ε>.

4.1 Three dimensional (3D) flow field

The computed 3D flow characteristics (U, k and $-\overline{uv}$) are presented in figures 5-10 for both arrangements (staggered and non-staggered) at characteristic planes, parallel to the channel bed, close to the top of vegetation.

Figures 5 and 6 show the velocity field at three planes for the staggered (Dunn et al., 1996) and non staggered arrangement (Poggi et al, 2004) respectively. The effect of vegetation (cylinders) on the velocity variation within a plane is clearly shown especially for the planes close to the top of vegetation. The magnitude of velocities in the first case (figure 5) is higher due to the higher bed slope.

Figures 7 and 8 show the k field at three planes for the two cases respectively. Again, the effect of cylinders on the turbulence field with increased values of k behind the cylinder (wake turbulence) especially at planes close to the top of cylinders. Similar conclusions can be derived from the shear stress fields (figures 9 and 10).

4.2 Spatial averaged flow field

Spatial averaged quantities have been calculated at various planes, parallel to the channel bed, using the relationship presented previously. The distribution of <U> within the flow depth is shown in figure 11 for the two arrangements (staggered and non staggered) and for different submergence ratio H/h and hence the effect of H/h on the <U> distribution within the flow depth can be studied. The velocity has been made dimensionless with the shear velocity at the interface ($U_* = \sqrt{g(H-h)S_o}$) and hence the velocity distribution above the vegetation can be compared with that over an impermeable (solid) wall. For both arrangements and for all H/h the velocity distribution is similar qualitatively. For the greater part of the vegetation layer, away from the channel bed and the interface, the distribution is uniform with a value equal to that derived from the balance between gravity forces and drag forces. Close to the interface, the velocity distribution is exponential with high velocity gradients while in the region above the vegetation the velocity seems to follow a logarithmic profile. The comparison of computed and experimental (Dunn et al., 2001) results for one case is satisfactory within the vegetation region, however, above the vegetation, the experimental velocities seem to be lower than the computed ones. The comparison of computed results with experimental ones of Poggi et al. (2004) for H/h=5 (the experimental profiles are based on local measurements) indicates that the experimental distribution is underestimated by the computations, but this may be due to the non full development of flow in the laboratory channel and the non-accurate estimate of the channel slope (1.26E-04). In figure 12 the dimensionless velocity $<U>/U_*$ is shown against the dimensionless distance $y+=((y-h)U_*/\nu)$ from the top of vegetation. In the same figure the log-law for flow over a solid wall is shown for comparison purposes. It is shown that the velocities under interacting conditions due to vegetation are much lower than those under isolated conditions (solid wall at the top of vegetation). The reduction of velocities is higher with increasing H/h.

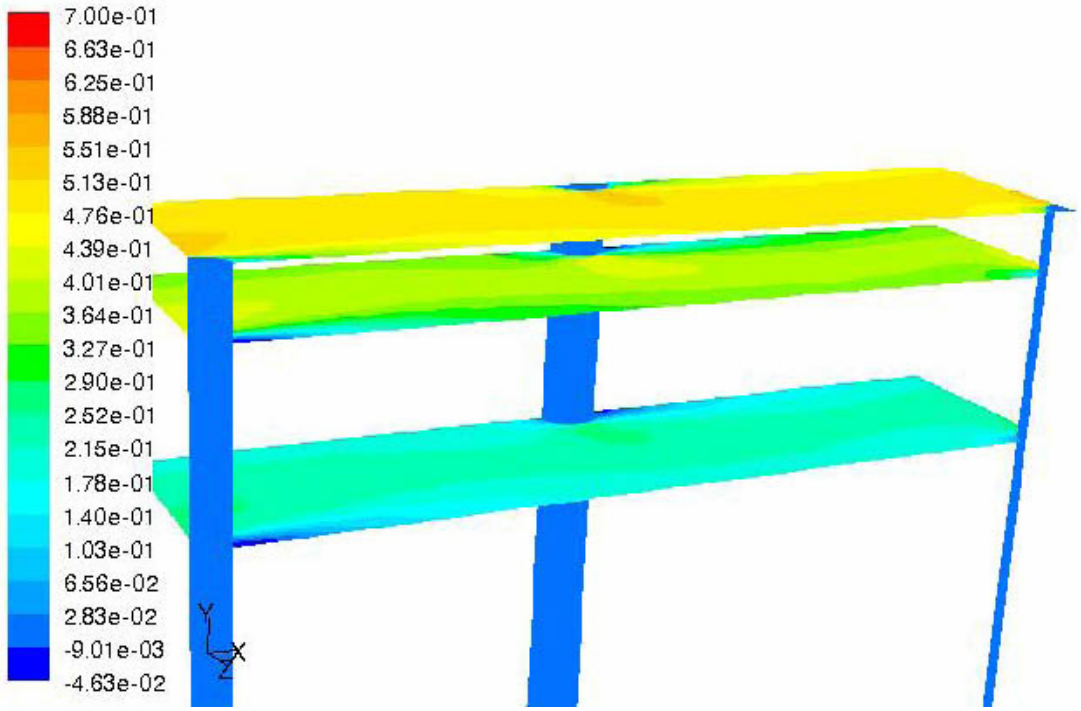

Figure 5: Velocity distribution at various planes within the vegetation (staggered)

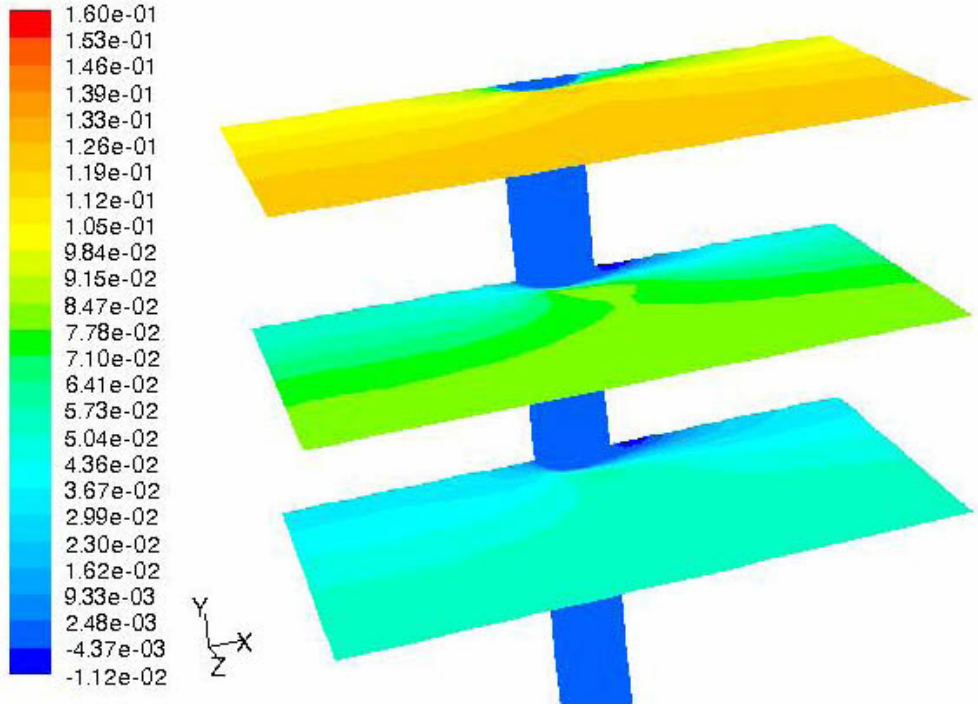

Figure 6: Velocity distribution at various planes within the vegetation (non-staggered)

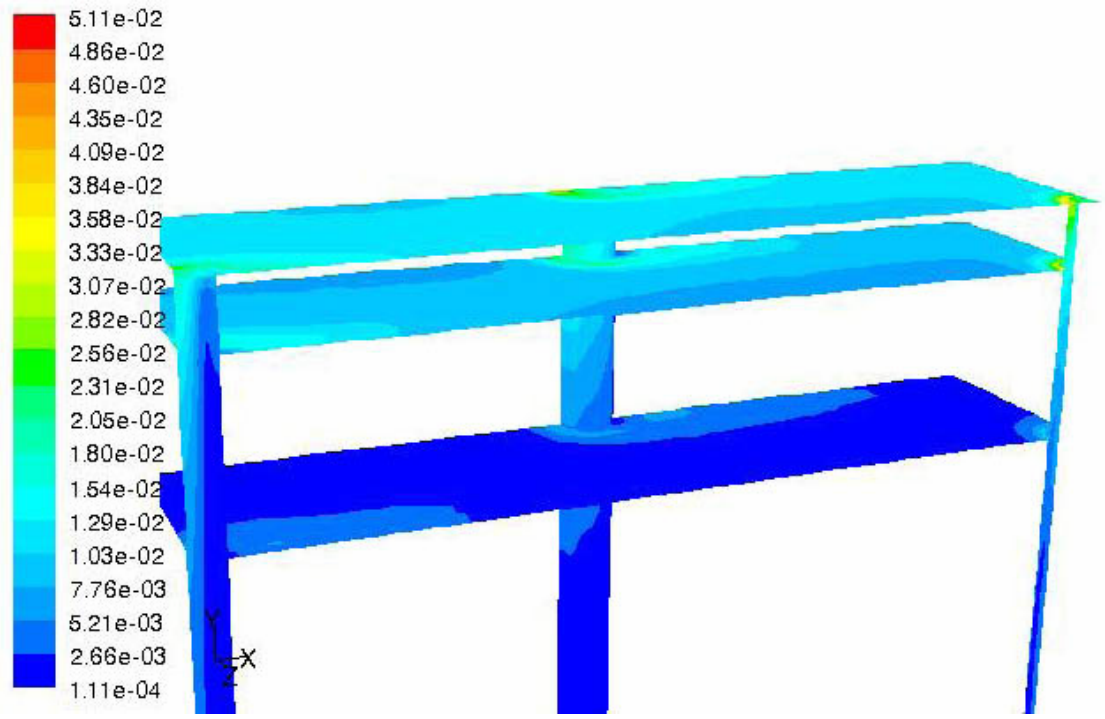

Figure 7: Turbulent Kinetic Energy distribution at various planes within the vegetation (staggered)

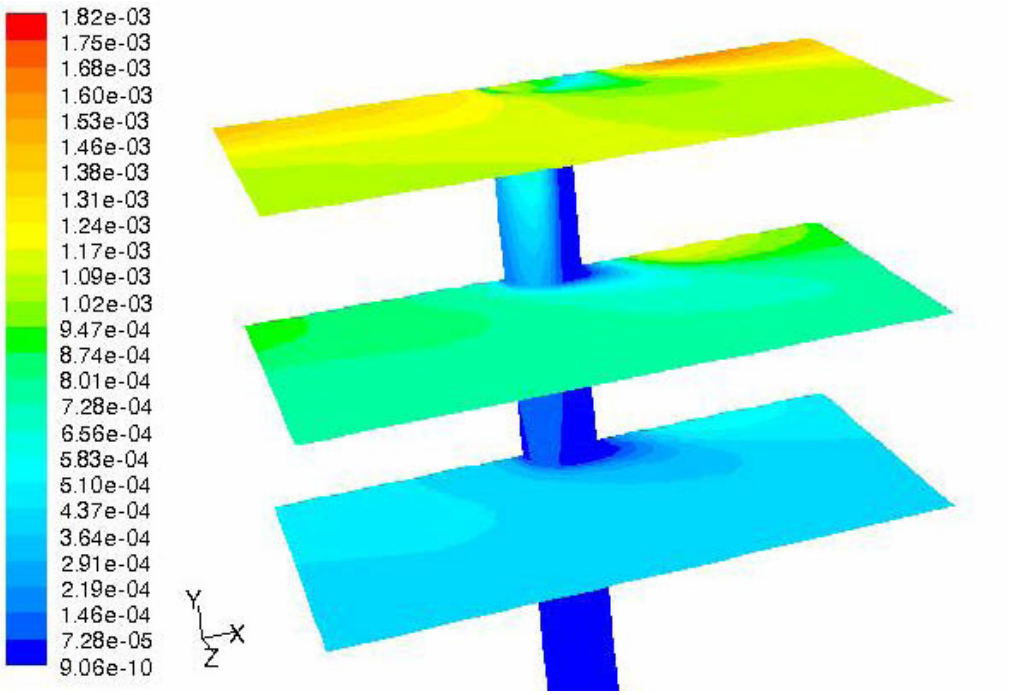

Figure 8: Turbulent Kinetic Energy distribution at various planes within the vegetation (non-staggered)

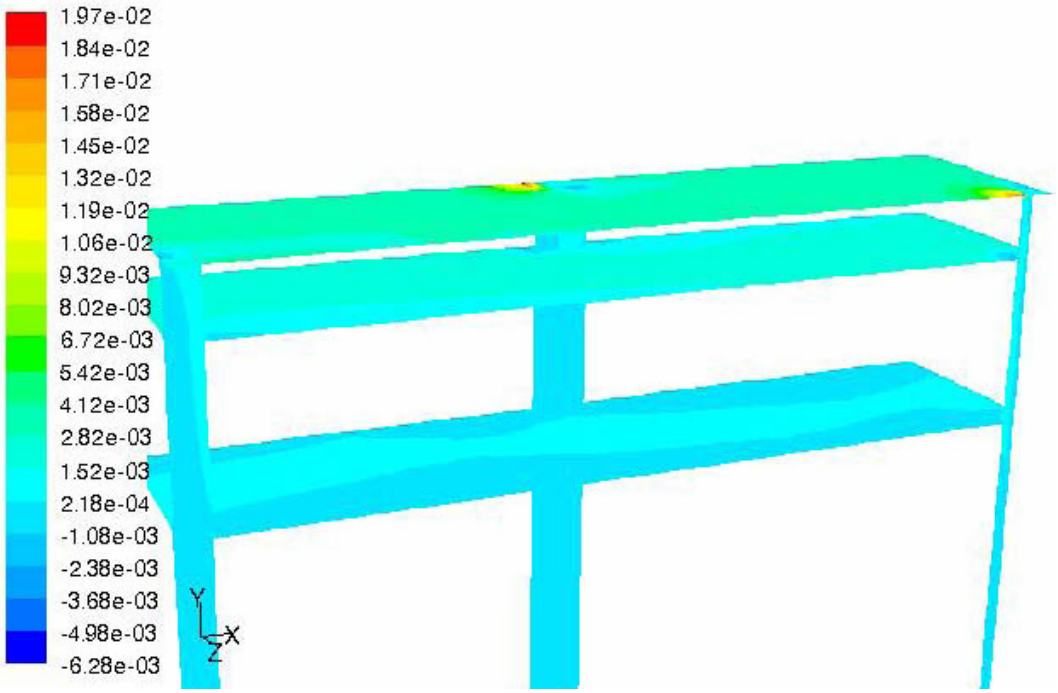

Figure 9: Reynolds stresses ($-\overline{uv}$) distribution at various planes within the vegetation (staggered)

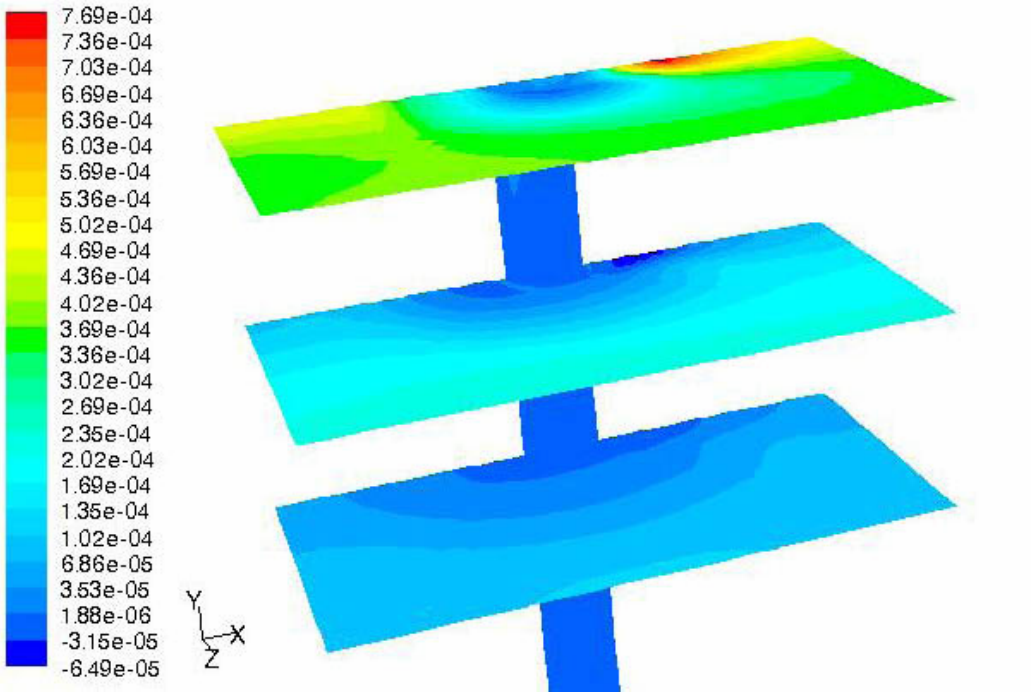

Figure 10: Reynolds stresses ($-\overline{uv}$) distribution at various planes within the vegetation (non-staggered)

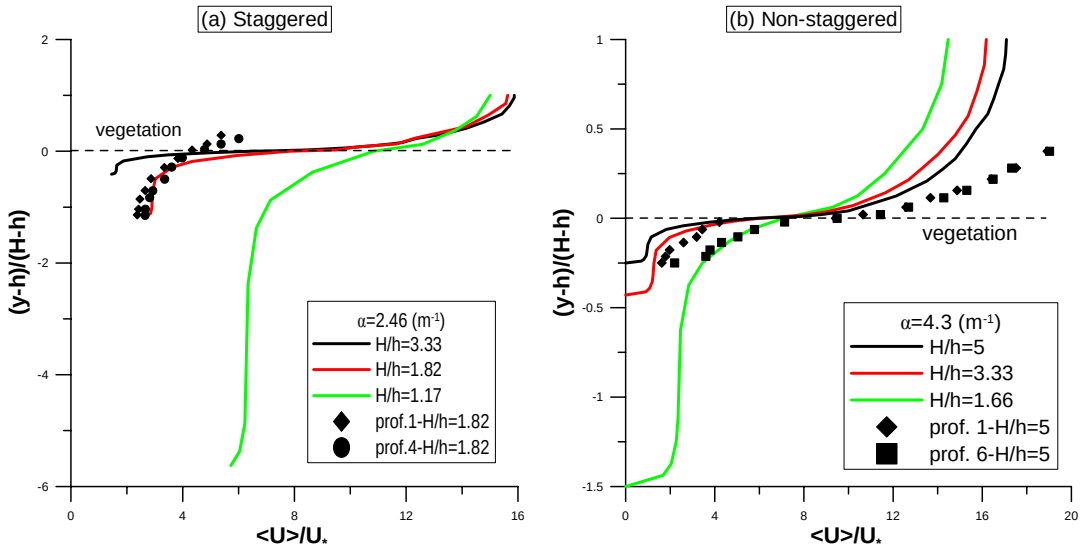

Figure 11: Distribution of <U>

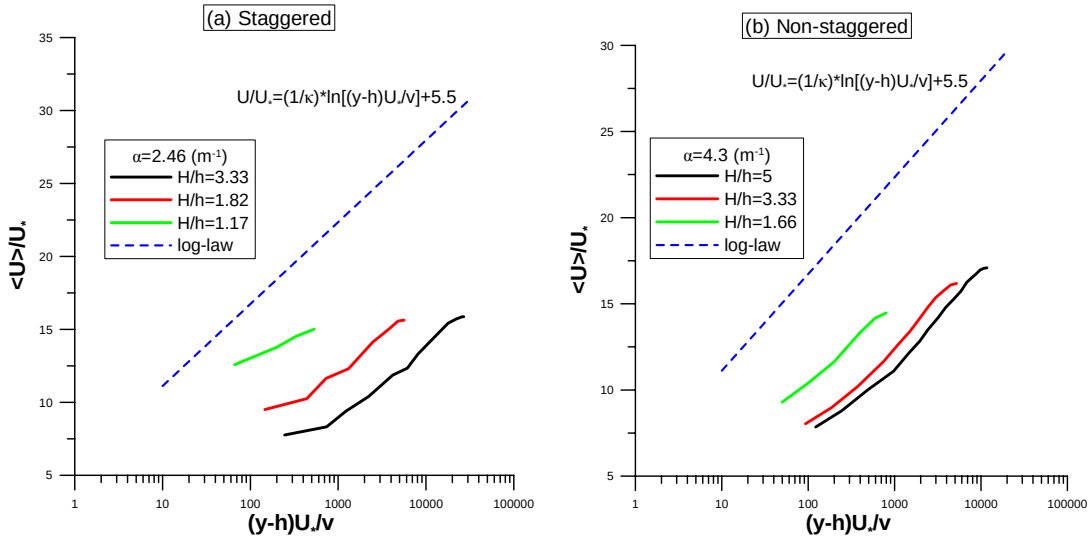

Figure 12: Logarithmic distribution of <U>

In figure 13 the distribution of $<-\overline{uv}>$ within the flow depth is shown. The shear stress has been made dimensionless with the U_*^2 and hence a comparison of the distribution of $<-\overline{uv}>$ above the vegetation with that over a solid wall is possible. It is shown that, for all H/h, the dimensionless shear stress varies from 1.0 (at the top of vegetation) to 0.0 (at the free surface) indicating that the shear velocity, based on the flow depth above the vegetation (H-h), is a characteristic variable which can be used for dimensional analysis purposes. Within the vegetation layer the shear stress takes values close to zero due to the uniform velocity distribution in this region. In cases with highly dense vegetation, the flow may become laminar in the central part of the layer and hence a low-Reynolds turbulence model would be appropriate for capturing the flow characteristics.

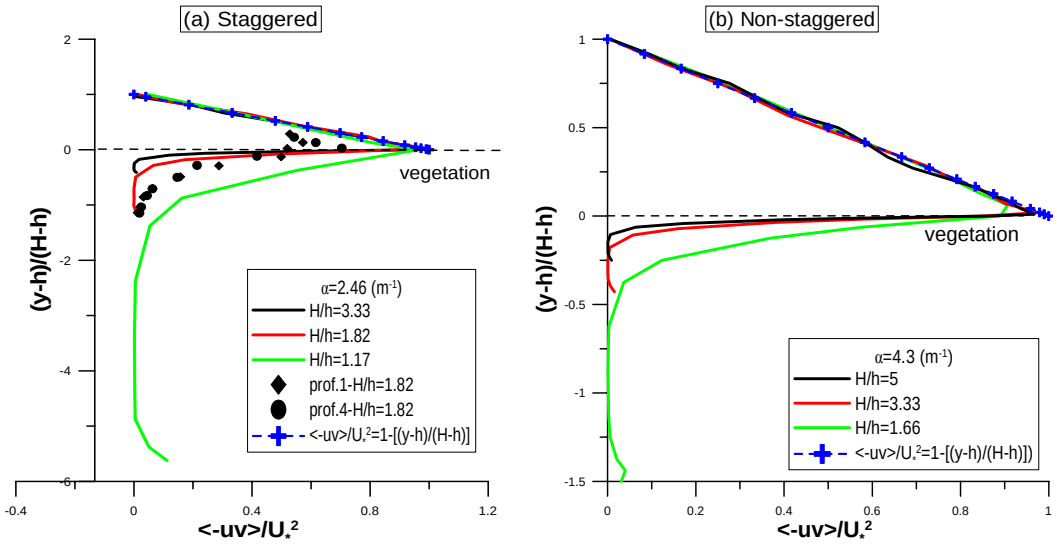

Figure 13: Distribution of $<-\overline{uv}>$

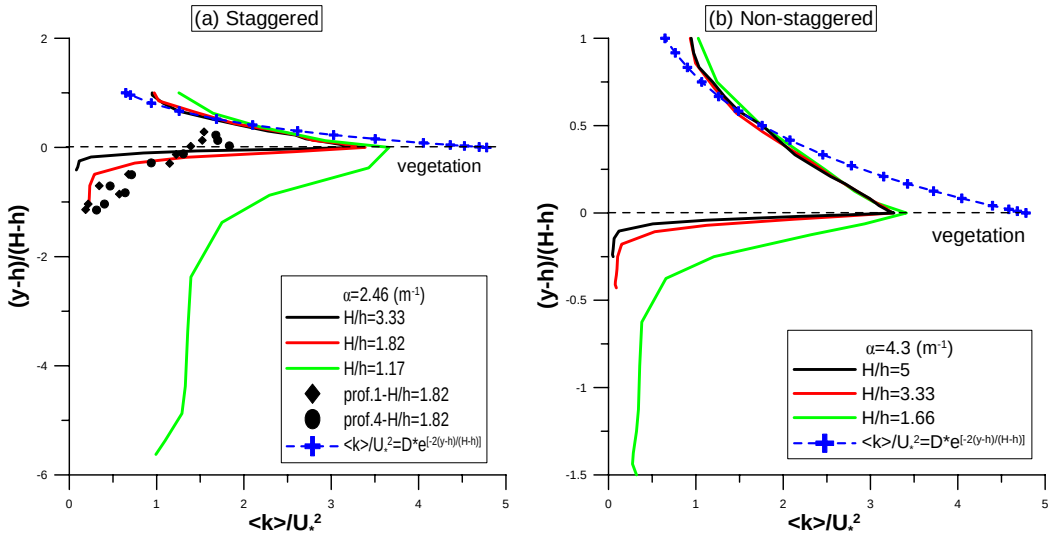

Figure 14: Distribution of <k>

In figure 14 the distribution of <k> is shown for the aforementioned cases together with experimental results and the semi empirical distribution of Nezu and Nakagawa (1993) for the distribution of k over a solid wall. The <k> levels at the top of vegetation (made dimensionless with U_*^2) are lower than the asymptotic value, D=4.7, of the semi-empirical relationship while above the vegetation the <k> values are similar to those of the semi-empirical relationship. Below the top of vegetation the <k> values remain high close to the top and fall suddenly to low values in the central part of the layer where turbulence is not considerable. The experimental values in the vegetation layer are comparable with the computed ones, however close and at the top of vegetation the values of <k> are lower in accordance with the low values of experimental velocities.

In figure 15 the distribution of turbulence intensity is shown. The square root of k, made dimensionless with the local <U>, shows a peak value within the vegetation region with levels up to 40% of the mean <U>, indicating an increased turbulent activity in the upper 50% of the vegetation layer. The computed distribution is in accord with measurements of $\sqrt{k}/<U>$ by Nepf and Vinoni (2000) who found a similar distribution with maximum values below the top of vegetation (Figure 7 of their paper). The maximum turbulence intensity decreases with decreasing depth ratio H/h.

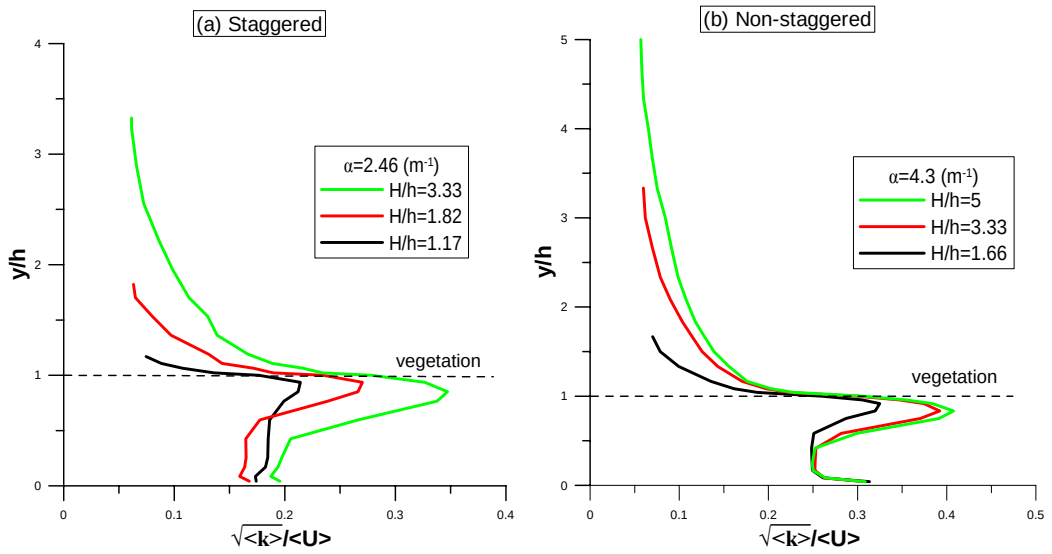

Figure 15: Distribution of $\frac{\sqrt{<k>}}{<U>}$

4.3 The Boussinesq Approximation for $<-\overline{u_i u_j}>$

Based on the Boussinesq approximation for determining the shear stress in a clear fluid, the respective volume averaged shear stress can be determined, with the use of Volume Average Theory (VAT) as

$$<-\overline{u_i u_j}>=<\nu_t>\cdot\left(\frac{\partial<U_i>}{\partial x_j}+\frac{\partial<U_j>}{\partial x_i}\right)+<\nu_t\frac{\partial U_i}{\partial x_j}>+<\nu_t\frac{\partial U_j}{\partial x_i}>-\frac{2}{3}\cdot<k>\cdot\delta_{ij} \qquad (11)$$

The second and third term in the rhs of the above equation include spatial fluctuation quantities which need modeling. In most volume-averaged turbulence models (Foudhil et al, 2005 and the references therein) these terms have been assumed negligible and hence the Boussinesq approximation was assumed valid for the spatial – averaged shear stresses.

The validation of this approximation was also tested in this study. The most significant shear stress $<-\overline{uv}>$, calculated by (11), is plotted in figure 16. Also, the shear stress $<-\overline{uv}>$ calculated directly from the microscopic values at the respective planes is included. It is shown that both distributions are in close agreement except in the region close to the top of vegetation where the two values are different. Hence, in most part of the vegetation layer and the surface layer the Boussinesq approximation for the spatial-averaged values holds. This is due to the low plant density (high porosity) in all these cases which results in negligible spatial variation of ν_t and velocity gradients and hence the

terms of eq. (11) with spatial fluctuations are very small. It is expected that for low porosities (high plant densities) these terms will be significant and further modeling will be required.

Finally, the relationship $\langle \nu_t \rangle = c_\mu \langle k \rangle^2 / \langle \varepsilon \rangle$ has been tested, since it used in all macroscopic turbulence models with a value of c_μ equal to 0.09 as in the microscopic models. Figure 17 indicates that such a value is not appropriate and a rather higher value (0.12-14) gives a better correlation between $\langle \nu_t \rangle$ and $\langle k \rangle^2 / \langle \varepsilon \rangle$.

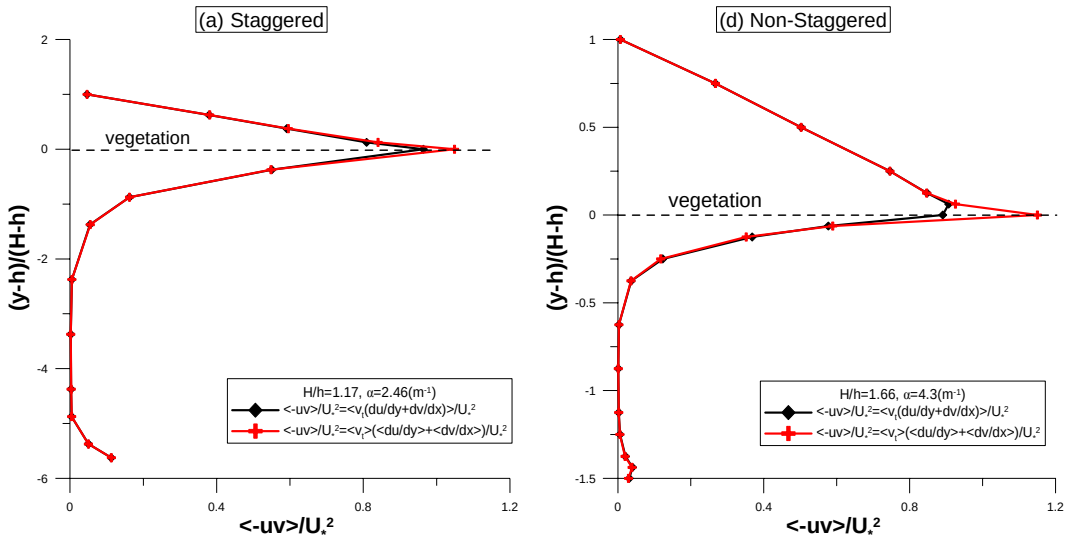

Figure 16: Validation of Boussinesq approximation for $\langle -\overline{uv} \rangle$

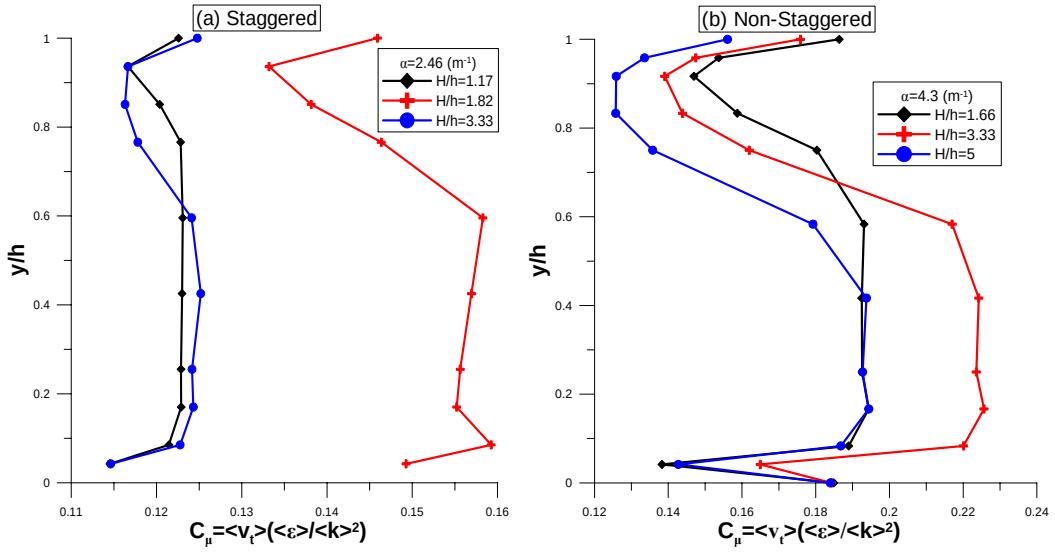

Figure 17: Variation of Cμ based on spatial-averaged quantities

5. Conclusions

Three-dimensional turbulent flow within and above submerged, rigid vegetation has been computed numerically using the 3D-RANS equations and a turbulence model of the k-ε type for submergence ratio H/h from 1.17 to 5.0, vegetation density from 2.46 to 4.3 and various staggered and non-staggered arrangements. Computed "micro" flow characteristics are used for calculating the respective "macro" spatial-averaged flow characteristics which are analyzed. Implications for the macroscopic modeling of such flows are discussed. The following conclusions can be derived:

(a) "Micro", three-dimensional flow characteristics (mean velocities, turbulence kinetic energy and shear stresses) indicate the effect of vegetation on the flow characteristics and in particular the increased turbulent activity in the wake of vegetation elements close to the top of vegetation.

(b) "Macro", spatial-averaged flow characteristics, calculated at characteristic planes, show distinct flow features within and above the vegetation region in comparison with flow characteristics over a solid wall.

(c) The Boussinesq approximation for the spatial-averaged shear stress $< -\overline{uv} >$ is found to be valid due to a rather low vegetation density (high porosity) of the cases examined.

(d) The relation between $<\nu_t>$ and turbulence quantities $<k>$ and $<\varepsilon>$ is tested and a higher value of c_μ (0.12-0.14) is recommended for use in macroscopic turbulence models of the $<k>$-$<\varepsilon>$ type.

REFERENCES

1. Choi, S.-U. and Kang, H., (2004) "Reynolds stress modeling of vegetated open channel flows", Journal of Hydraulic Research, IAHR, 42, 3-12.
2. Dunn, C., López, F. and García, M.H., (1996) "Mean flow and turbulence in a laboratory channel with simulated vegetation vegetation", Civil Engineering Studies, Hydraulic Engineering Series No. 51
3. Finnigan, J.J. (2000) "Turbulence in plant canopies", Annu. Rev. Mech.,32, 519-571
4. FLUENT INC. (2001) "Fluent 6.0 Documentation", Lebanon, USA.
5. Foudhil, H., Brunet, Y. and Caltagirone, J.-P., (2005) "A Fine-Scale k-ε Model for Atmospheric Flow over Heterogeneous Landscapes", Enviromental Fluid Mechanics (2005) 5: 247-265
6. Huthoff, F. and Augustijn, D.(2006) "Hydraulic resistance of vegetation: Predictions of average flow velocities based on a rigid-cylinders analogy", Final Project Report, Planungsmanagement fur Auen (Project no.U2/430.9/4268)
7. Neary, V.S. (2003) "Numerical Solution of Fully Developed Flow with Vegetative Resistance", Journal of Engineering Mechanics ASCE
8. Nepf, H.M. and Vivoni, E.R. (2000) "Flow structure in depth-limited, vegetated flow", J. of Geophysical Research, AGU, 105(C12), pp. 28547-28557.
9. Nezu, I. and Nakagawa, H., (1993) "Turbulence in open-channel flows", IAHR Monograph, Balkema, Rotterdam, The Netherlands
10. Poggi, D., Porporato, A., Ridolfi, L., Albertson, D.-J. and Katul G.-G. (2004) "The effect of vegetation density on canopy sub-layer turbulence", Boundary-Layer Meteorology 111:565-587, 2004
11. Rodi, W. (1980) "Turbulence Models in Hydraulics ", IAHR Publication, Delft, The Netherlands.
12. Whitaker, S. (1999) "The method of volume averaging", Kluwer Academic Publishers, Dordrecht